

Exploring Low Internal Reorganization Energies for Silicene Nanoclusters

Ricardo Pablo-Pedro,¹ Hector Lopez-Rios,² Jose-L. Mendoza-Cortes,^{3,4} Jing Kong,⁵
Serguei Fomine,² Troy Van Voorhis,^{1,*} and Mildred S. Dresselhaus^{5,6,†}

¹*Department of Chemistry, Massachusetts Institute of Technology,
77 Massachusetts Avenue, Cambridge, Massachusetts 02139, USA*


²*Instituto de Investigaciones en Materiales, Universidad Nacional Autónoma de México,
Apartado Postal 70-360, CU, Coyoacán, Ciudad de México 04510, México*

³*Department of Chemical and Biomedical Engineering, FAMU-FSU Joint College of Engineering,
Tallahassee, Florida 32310, USA*

⁴*Department of Physics and Department of Scientific Computing, Materials Science and Engineering,
High Performance Material Institute, Condensed Matter Theory,
National High Magnetic Field Laboratory, Florida State University, Tallahassee, Florida 32310, USA*

⁵*Department of Electrical Engineering and Computer Science, Massachusetts Institute of Technology,
Cambridge, Massachusetts 02139, USA*

⁶*Department of Physics and Department of Electrical Engineering and Computer Science,
Massachusetts Institute of Technology, Cambridge, Massachusetts 02139, USA*

 (Received 15 August 2017; revised manuscript received 11 February 2018; published 9 May 2018)

This paper is a contribution to the [Physical Review Applied](#) collection in memory of Mildred S. Dresselhaus.

High-performance materials rely on small reorganization energies to facilitate both charge separation and charge transport. Here, we perform density-functional-theory calculations to predict small reorganization energies of rectangular silicene nanoclusters with hydrogen-passivated edges denoted by H-SiNC. We observe that across all geometries, H-SiNCs feature large electron affinities and highly stabilized anionic states, indicating their potential as *n*-type materials. Our findings suggest that fine-tuning the size of H-SiNCs along the “zigzag” and “armchair” directions may permit the design of novel *n*-type electronic materials and spintronics devices that incorporate both high electron affinities and very low internal reorganization energies.

DOI: [10.1103/PhysRevApplied.9.054012](https://doi.org/10.1103/PhysRevApplied.9.054012)

I. INTRODUCTION

Graphene has attracted increasing interest since the discovery of its potential as a future elementary unit in modern microelectronics such as field-effect transistors [1], photovoltaic cells [2], advanced gas sensors [3], and battery energy storage [4]. Additionally, the isolation of graphene has inspired the new world of two-dimensional (2D) materials, where some recent members include black phosphorus [5], transition-metal dichalcogenides (TMDs) [6], and silicene [7]. Among these 2D materials, silicene has been predicted to possess most of the remarkable electronic properties of graphene, such as a Dirac cone, carrier mobility, and high Fermi velocity [7]. Moreover, the major advantage of investigating silicene is that it can be easily incorporated into the present silicon-based microelectronics industry [8,9]. In this direction, considerable

improvements have been achieved in the use of silicene as field-effect transistors at room temperature [10] and in spintronics applications [11].

Interestingly, the electronic properties of silicene change in a nontrivial manner when going to lower dimensions. Silicene nanoribbons, for instance, can be either metals or semiconductors depending on their width [9]. For the case of silicene nanoclusters, the electronic structure is expected to be different from pristine silicene and nanoribbons because there are additional degrees of freedom from the edge atoms [8]. In addition, silicene nanoclusters have the advantage that they all possess fine band gaps because of the quantum-confinement effect that is desirable for their applications. The fabrication of these silicene nanostructures can be realized using etching techniques that have been already used in cutting graphene sheets into nanostructures with desired shape and size. This experimental progress motivates our study of the electronic structure of silicene nanoclusters with rectangular shape [12,13].

Carrier transport is the central property for applications of silicene in field-effect transistors, thermoelectric devices,

*To whom all correspondence should be addressed.
tvvan@mit.edu

†Deceased.

and spintronics. Therefore, having high carrier mobility is very important for developing new silicene nanoelectronic devices. The transport mechanism is generally understood with respect to the limiting cases of hopping (polaron) transport and bandlike transport corresponding to the extreme localization or delocalization of the charge carriers. The bandlike regime is generally observed only at low temperatures in highly ordered samples (i.e., the mobility μ decreases with the temperature as $\mu \propto T^{-n}$) up to room temperature [14]. The hopping (polaron) mechanism consisting with the carrier is localized on one molecule, through the formation of a self-trapped state (a polaron) and transport occurs through a thermally activated hopping mechanism (strong electron-phonon coupling), which is observed commonly in small molecules and molecular semiconductors at high temperatures [15]. For instance, the electron-phonon interaction of silicene is considerable, as the larger Si-Si interatomic distance of silicene compared to graphene weakens the π - π overlaps and results in a low-buckled structure with sp^3 -like hybridization [7]. Then, because of the size of our silicene nanocluster and large geometry relaxations of the silicene nanoclusters, we consider that they can be described by the hopping mechanism in which the mobility (μ) of the charge carriers (electrons or holes) is directly proportional to the transfer rate (k) of charge carriers described by the Einstein relation [16]

$$\mu = \frac{eA^2}{k_B T} k, \quad (1)$$

where k_B , T , e , and A are the Boltzmann constant, temperature, electron charge, and hopping transport distance, respectively. According to the Marcus-Huss semiclassical model for the interchain charge transfer, the charge-transfer rate is given by [16]

$$k = \frac{2\pi}{h} \left(\frac{\pi}{\lambda k_B T} \right)^{-1/2} H_{ab}^2 e^{-[\lambda/(4k_B T)]^2}. \quad (2)$$

Here h , λ , and H_{ab} are the Planck constant, the reorganization energy, and the electronic coupling matrix element between the donor and acceptor, respectively. According to Eq. (2), the charge transfer is determined by H_{ab} and λ . However, H_{ab} starts to saturate for oligomers with more than five monomeric units indicating the exponential contribution in Eq. (2) keeps increasing, and for more than seven monomeric units, it dominates the behavior of the charge-transfer rate [17]. Therefore, the key parameter that governs the behavior of the charge-transfer rate is the reorganization energy which decreases with an increasing length of the system, as we discuss below. At some point, the transfer coupling is expected to saturate once it depends on the conjugation length of the polymers [16]. Then, for large conjugated polymers and organic

molecular semiconductors, the exponential nature of Eq. (2) dominates, and in this way, the reorganization energy is the most important parameter to be studied to estimate the charge carrier transport. The reorganization energy λ corresponds to the energy of structural change when going from neutral-state geometry to charged-state geometry and vice versa. In terms of the electron-phonon mechanism, λ is a measure of the strength of the electron-phonon interaction and produces a relation between the geometry, electronic structure, and transport properties of the material [18]. The reorganization energy can be divided in terms of the transport of holes (λ_+) and electrons (λ_-) in order to determine whether a material may have a greater mobility of electrons than holes or of holes than electrons, respectively. It is known that most organic semiconductors have hole reorganization (λ_+) energies greater than 0.1 eV; however, several hole-transporting (p -type) organic semiconductors have been reported with hole reorganization energies of less than 0.1 eV, for example, pentacene (0.097 eV) [19] and circum (oligo)acenes (0.057 to 0.127 eV) [20]. On the other hand, studies of electron-transporting (n -type) semiconductors have been limited in the last decade because of the instability in air of radical anionic semiconductors and the high injection barrier of electrons. One of the few examples is fullerene (C_{60}), which has been found to be an excellent n -type acceptor with a small electron reorganization energy of $\lambda_- = 0.060$ eV [21]. This small reorganization energy allows fast photoinduced charge separation and slow charge recombination resulting in the formation of a long-lived charge-separated state with high quantum yield [22]. The small reorganization energy of fullerene can also be ascribed to its extended π conjugation and its rigid molecular structure. In general, the hole (λ_+) and electron (λ_-) reorganization energy decreases as the size of the π -conjugated system is increased. For instance, anthracene $\lambda_+ = 0.137$ eV and $\lambda_- = 0.196$ eV, tetracene 0.113 and 0.160 eV, and pentacene 0.097 and 0.132 eV [23], respectively.

In anisotropic 2D semiconductors such as TMDs [24,25], black phosphorus [26,27], and silicone [8], the electrons and phonons behave differently in different in-plane directions, e.g., armchair and zigzag directions. This anisotropic behavior leads to angle-dependent mechanical, optical, and electrical responses. Therefore, we hypothesize that the reorganization energies in anisotropic materials should exhibit different behaviors along different directions. These unique properties may permit the design of novel electronics and optoelectronics with anisotropic crystalline orientation.

In this work, we study the reorganization energies of rectangular silicene nanoclusters with hydrogen-passivated edges (H-SiNCs) along different directions by using density-functional theory (DFT). The values of the reorganization energies for H-SiNCs are obtained by varying the

width of the zigzag and the armchair directions. To further evaluate these H-SiNCs, we compute the adiabatic electron affinities (EAs) and the ionization potential (IP) energies.

II. COMPUTATIONAL DETAILS

We carry out geometrical optimizations of rectangular silicene nanoclusters utilizing the three-parameter Becke and Lee-Yang-Parr functional (B3LYP) in conjunction with Dunning's correlation-consistent polarized valence, double-zeta (cc-pVDZ) basis set for all atoms. For all molecules, we use restricted DFT (RB3LYP) or unrestricted DFT (UB3LYP) when specified. Grimme's *D3* dispersion correction [28] is also used in all DFT calculations to account for the dispersion interactions. Thus, the methods are named RB3LYP-*D3* and UB3LYP-*D3*; we indicate in the text if only one method is used. The need for UB3LYP-*D3* is due to the singlet-triplet instability detected in the model's optimized closed-shell singlet-state wave function, also necessitating the consideration of two different values of multiplicities, singlet and triplet states. Here, a singlet state is an electronic state such that all electron spins are paired (antiferromagnetic state), while in a triplet state, the electron that is promoted has the same spin orientation (parallel) to the other unpaired electron (ferromagnetic state). Singlet and triplet spin values are derived using the equation for multiplicity $2S + 1$, where S is the total spin angular momentum (sum of all electron spins in the molecule). The closed-shell singlet systems that present triplet instability are reoptimized using the unrestricted-broken-symmetry method [29]. Additionally, the frequency calculations for the selected H-SiNCs are performed to ensure the absence of any vibrational instabilities in the ground-state structures. None of the systems analyzed have negative frequencies, which means that they are thermodynamically stable. The calculations are performed using the code TURBOMOLE v7.0 [30]. From here on, we denote the UB3LYP-*D3* method as B3LYP for simplicity.

We also run complete active-space self-consistent-field (CASSCF) calculations of the charged molecules of the corresponding electronic multiplicity also using the B3LYP functional to explore their multiconfigurational character. This is to correct and compare, if needed, for the multiconfigurational character of the neutral H-SiNCs reported in a previous study [8] at the B3LYP level of theory. In addition, we run CASSCF calculations in order to revise the correlation between the UB3LYP and the CAS level of theory [31]. They both show that anionic species are the most stable species compared with the cationic species as shown in the Supplemental Material [31]. Hence, the computations for the silicene nanoclusters at complete active-space self-consistent field-level support the conclusions obtained at the DFT level. The chosen active spaces consist of nine electrons and ten orbitals, and 11 electrons and ten orbitals, for cation and anion radicals, respectively. The selection of the active space is simple, since all π

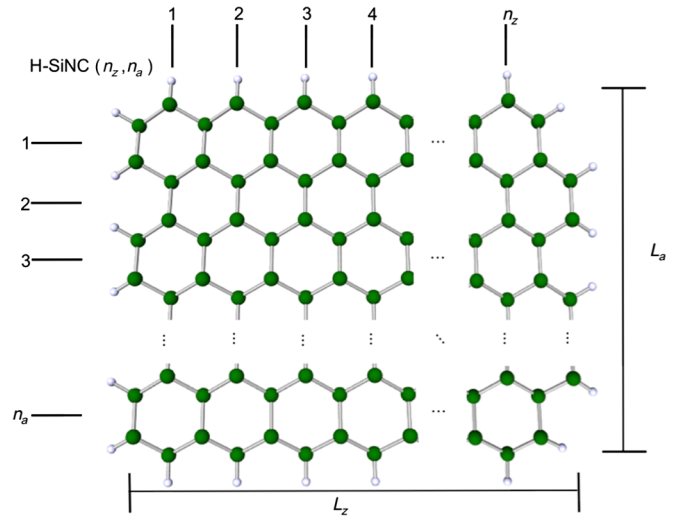


FIG. 1. Top-down view of a lattice structure of silicene, where the edges are passivated with hydrogen. n_z and n_a are the number of fused benzene rings in columns and rows.

orbitals form the correct active space, the more orbitals one includes the better its description. We include as many orbitals as possible from the computational point of view. Since most of the systems have only two or three important configurations, we use an active space consisting of more than 100 000 configurations that seems to be adequate from our point of view. In addition, we visualize the corresponding orbitals to ensure that they involve all atoms of the studied systems, and we inspect the density matrix generated in each calculation to ensure that all active orbitals have population numbers between 0.1 and 1.9, a confirmation of a correctly selected active space. The 6-31G(d) basis set is assigned to all atoms. These calculations are carried out with Gaussian 09 rD.01. code [32].

We study rectangular silicene nanoclusters following the pattern shown in Fig. 1. All edge dangling bonds are passivated with hydrogen. To specify the size of each H-SiNC, we use n_z and n_a , which correspond to the number of hexagonal units along the zigzag and armchair edges. Here, we define a characteristic area scale by $N = n_z \times n_a$, which corresponds to the total of fused rings in the silicene nanocluster. The characteristic dimensions of each H-SiNC are denoted here by L_a (armchair edge) and L_z (zigzag edge) being linear functions of n_a and n_z and the average Si—Si bond length. We vary n_a from 1 to 9 (which means that L_a varies from 0.439 nm for $n_a = 1$ to 3.112 nm for $N = 9$, approximately) and for n_z from 1 to 7 (L_z varying from 0.381 nm for $n_z = 1$ to 2.882 nm for $n_z = 7$).

The geometry of every silicene nanocluster is first optimized for the neutral molecule at the B3LYP level, $E_0(q_0)$. The energy is then calculated for the negatively charged molecule (adding an electron to the neutral molecule) in the optimized geometry of the neutral molecule, $E_-(q_0)$. The geometry of the negatively charged molecule is subsequently optimized to obtain $E_-(q_-)$.

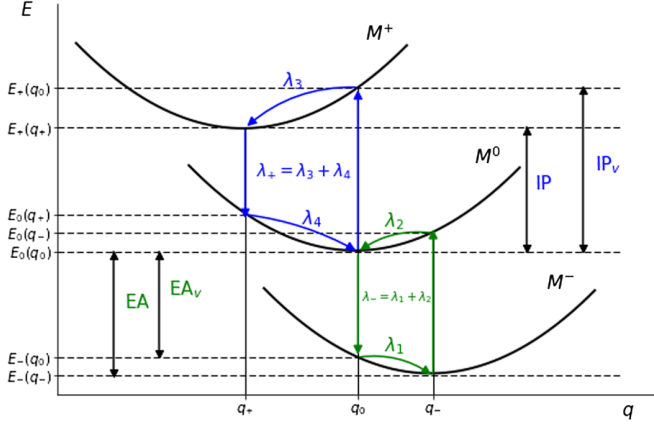


FIG. 2. Potential energy surfaces sketch for the neutral (M^0), negatively (M^-), and positively (M^+) charged structures. E is the energy, q is the geometry, and the subscripts 0, $-$, and $+$ denote neutral, anionic, and cationic states, respectively. Here, IP is the ionization potential, EA is the electron affinity, and the subscript v denotes vertical energy transitions.

Their energy difference $E_-(q_0) - E_-(q_-)$ is equal to the reorganization energy λ_1 ; see Fig. 2. We now remove an electron from the optimized negatively charged molecule and calculate the energy without relaxing the geometry to obtain the $E_0(q_-)$ state. The energy difference between the $E_0(q_-)$ state and the optimized neutral molecule $E_0(q_0)$ is the reorganization energy λ_2 , as shown in Fig. 2. Then, the total electron reorganization energy for the process is equal to [33]

$$\lambda_- = \lambda_2 + \lambda_1 = [E_0(q_-) - E_0(q_0)] + [E_-(q_0) - E_-(q_-)], \quad (3)$$

where E is energy and q is the geometry. The subscripts 0 and $-$ represent the neutral and anionic states, respectively. The same procedure is carried out for the cation state. Thus, the hole reorganization energy is given by [33]

$$\lambda_+ = \lambda_4 + \lambda_3 = [E_0(q_+) - E_0(q_0)] + [E_+(q_0) - E_+(q_+)]. \quad (4)$$

Here, E is energy and q is the geometry as in Eq. (3). The subscripts 0 and $+$ represent the neutral and cationic states, respectively. Moreover, we use the total-energy differences between the DFT B3LYP calculations performed for the neutral and charged systems to evaluate (i) the adiabatic IPs and EAs and (ii) the highest occupied molecular orbital (HOMO) and lowest unoccupied molecular orbital (LUMO) energies for the neutral systems. The vertical transitions involved in Eqs. (3) and (4) are shown in Fig. 2.

III. RESULTS AND DISCUSSION

We summarize the optimized bond lengths of ground, cationic, and anionic states for selected H-SiNC(n_z, n_a) in Table I at the B3LYP or cc-pVDZ level of theory. Two multiplicities are used according to previous results, i.e., single ($S = 0$) and triplet ($S = 1$). The bond-length increases (decreases) going from the neutral to the negatively (positively) charged structure show a consistent trend along the series. Overall, small molecules show the largest geometry relaxations, e.g., H-SiNC(2,1) changes its Si—Si bond lengths approximately 0.025 Å. This value is reduced to 0.005 and 0.002 Å in H-SiNC(7,1) and H-SiNC(5,4), respectively. However, the geometry distortions in the buckled structure of the silicene nanoclusters are larger than in the Si—Si bond lengths with averaged differences in the range of ± 0.03 Å, indicating that even for a large system, e.g., H-SiNC(5,4), the neutral molecule suffers large height modifications in its charged species, as shown in Fig. 3. Compared to the neutral geometry, the cationic geometry shrinks via the shortening of both bonds and heights, and the anionic geometry expands via lengthening of the bonds and heights. These geometry distortions (i.e., bond lengths and heights) of the H-SiNCs can explain why in some silicene nanoclusters the small reorganization energies are small (see the Supplemental Material [31]). In terms of π conjugation, larger silicene nanoclusters possess an extensive π conjugation that leads to greater delocalized charge distribution. Thus, local structural adjustment (i.e., bond length and height) for electron transfer (λ_-) is less severe in large silicene systems than smaller systems; see the Si—Si bond lengths and heights (Δ_a) in Table I.

TABLE I. The average Si—Si bond lengths (d_a) and the average height (Δ_a) of selected neutral, cationic, and anionic silicene structures at the B3LYP level of calculation. Here, the subscripts 0, $+$, and $-$ represent the neutral, cationic, and anionic states, respectively, and S represents the initial triplet and singlet states.

H-SiNC(n_z, n_a)	S	d_a^0 (Å)	d_a^+ (Å)	d_a^- (Å)	Δ_a^0 (Å)	Δ_a^+ (Å)	Δ_a^- (Å)
(2,1)	0	2.254	2.251	2.279	0.459	0.396	0.572
(7,1)	0	2.264	2.260	2.269	0.441	0.420	0.479
(5,4)	0	2.271	2.269	2.273	0.480	0.467	0.489
(4,7)	0	2.272	2.270	2.273	0.482	0.473	0.487
(4,9)	0	2.272	2.271	2.273	0.480	0.475	0.484
(4,9)	1	2.272	2.271	2.273	0.480	0.474	0.488

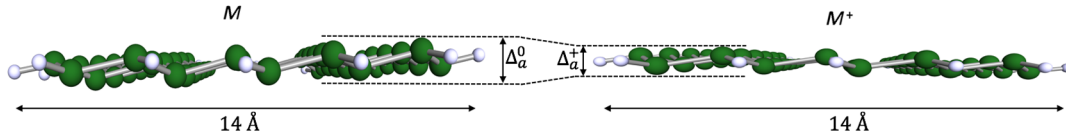


FIG. 3. Neutral state (left) of H-SiNC(5,4) relaxes into a new structure (right) when one electron is removed. As a result, the silicene nanocluster contracts along the vertical axis. The displacement is magnified 2 times in order to make this distortion clear.

In general, for the H-SiNCs, the largest structural changes are observed in the average height of the anions.

We summarize the calculated hole (λ_+) and electron (λ_-) reorganization energies and the adiabatic values of the EA and IP for the rectangular silicene nanoclusters in Table II at the B3LYP level of study. It is demonstrated that the B3LYP functional used for the reorganization energy calculations best reproduces the experimental data for conjugated organic systems [34,35]. In addition, the B3LYP functional is found to reproduce reliable EAs for 14 atoms and 96 molecules [36].

The adiabatic IPs and EAs presented in Table II are computed from the difference in the total energy between the

TABLE II. Hole (λ_+) and electron (λ_-) reorganization energies along with their adiabatic IPs and EAs calculated at the B3LYP level of theory. Here, S_{initial} represents the initial triplet and singlet states.

H-SiNC(n_z, n_a)	N	S_{initial}	λ_- (eV)	EA (eV)	λ_+ (eV)	IP (eV)
(1,1)	1	0	0.775	1.39	0.303	7.12
(2,1)	2	0	0.297	1.93	0.182	6.47
(3,1)	3	0	0.237	2.39	0.148	6.06
(4,1)	4	0	0.121	2.68	0.117	5.80
(5,1)	5	0	0.088	2.85	0.099	5.66
(6,1)	6	0	0.078	2.94	0.094	5.59
(7,1)	7	0	0.077	2.99	0.093	5.56
(2,2)	4	0	0.315	2.38	0.144	6.06
(3,2)	6	0	0.233	2.73	0.117	5.75
(4,2)	8	0	0.136	2.95	0.101	5.56
(5,2)	10	0	0.114	3.05	0.100	5.48
(6,2)	12	0	0.134	3.10	0.105	5.46
(7,2)	14	0	0.159	3.13	0.099	5.47
(3,3)	9	0	0.142	2.91	0.085	5.57
(4,3)	12	0	0.091	3.09	0.077	5.42
(5,3)	15	0	0.143	3.15	0.086	5.40
(6,3)	18	0	0.190	3.19	0.133	5.40
(7,3)	21	0	0.205	3.21	0.090	5.38
(4,4)	16	0	0.081	3.19	0.072	5.33
(5,4)	20	0	0.220	3.22	0.083	5.34
(6,4)	24	0	0.188	3.24	0.138	5.34
(7,4)	28	0	0.150	3.28	0.075	5.29
(4,5)	20	0	0.067	3.26	0.063	5.27
(4,6)	24	0	0.287	3.31	0.065	5.22
(4,7)	28	0	0.076	3.35	0.070	5.18
(4,8)	32	0	0.214	3.39	0.066	5.15
(4,9)	36	0	0.181	3.41	0.206	5.12
(4,7)	28	1	0.069	3.09	0.065	5.14
(4,8)	32	1	0.062	3.16	0.059	5.12
(4,9)	36	1	0.088	3.19	0.052	5.10

optimized neutral state and the corresponding optimized cation or anion state, i.e., $\text{IP} = E_+(q_+) - E_0(q_0)$ and $\text{EA} = E_0(q_0) - E_-(q_-)$ [37]. For all studied H-SiNCs, the cationic state potential energy is higher than the neutral-state potential energy giving a positive IP. Moreover, it is observed that the IPs of the H-SiNCs drop with the number of fused rings N , which is in agreement with other conjugated systems. In the case of the EAs, all H-SiNCs bind an electron with a positive EA, which also increases along with the number of benzoic rings. For n -type organic semiconductors, the adiabatic EA is an important property that determines organic field-effect transistor device performance such as durability. Among the studied systems, a few H-SiNCs exhibit quite large adiabatic EAs, exceeding the threshold of 2.80 eV used for classifying n -type materials [38,39]. Hence, H-SiNCs are expected to be stable electron-transport materials [40].

As seen in Table II, almost all of the H-SiNCs have a larger λ_- value than λ_+ . Contextualizing our results, linear silicene nanoclusters can be considered as analogous molecules with oligoacenes. For instance, we compare some λ_+ values of linear H-SiNCs with some common polycyclic aromatic hydrocarbons, i.e., C_{10}H_8 ($N = 2$), $\text{C}_{14}\text{H}_{10}$ ($N = 3$), $\text{C}_{18}\text{H}_{12}$ ($N = 4$), and $\text{C}_{22}\text{H}_{14}$ ($N = 5$) at the B3LYP 6-31G** level of theory, which are 0.187, 0.137, 0.113, and 0.097 eV [12], respectively. These values are comparable to the corresponding silicene systems H-SiNC(2,1), 0.182 eV; H-SiNC(3,1), 0.148 eV; H-SiNC(4,1), 0.117 eV; H-SiNC(5,1), 0.099 eV at the B3LYP level of theory. For some H-SiNCs, their hole and electron reorganization energies are less than 0.1 eV, such as H-SiNC(4,5) and H-SiNC(4,7). For systems with an initial triplet ground state, we can obtain even smaller hole and electron reorganization energies that can be compared to fullerene (0.06 eV). These low values suggest that the mobility along the armchair direction is greater than in the zigzag direction for these systems, with $n_a > n_z$. In addition, we can observe that the values of λ_- and λ_+ for systems with an initial triplet ground ($S = 1$) state are similar. This similarity in the electron and reorganization energies may suggest that these specific systems can act as ambipolars or n -acceptor materials merely considering the calculated electron and hole reorganization energies and adiabatic EA values. From these results, it can be concluded that the initial ground state's spin state of the H-SiNCs has a profound effect on the reorganization energy as seen for H-SiNC($4, n_a$), with $n_a = 7-9$.

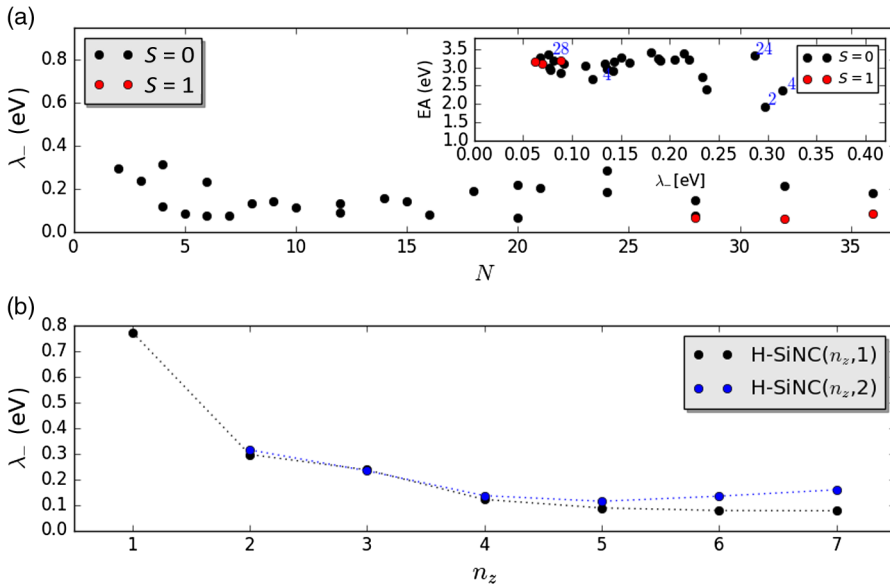


FIG. 4. (a) Plot of electron reorganization versus the number of fused rings N for H-SiNCs. Here, S represents the initial spin for the triplet and singlet states for $S = 1$ and $S = 0$, respectively. Inset: Plot of EA versus electron reorganization energy (λ_-). The numbers in the graph indicate the number of fused rings (N) for selected H-SiNCs. (b) Plot of the electron reorganization energy versus the number of fused rings along the zigzag direction for H-SiNCs with a singlet ground state.

To examine the effect of the number of fused rings on the electron transfer, λ_- is plotted for different H-SiNCs in Fig. 4(a). Since we are comparing different orientations (i.e., armchair and zigzag directions), there is not a perfect relationship between electron reorganization energy and the number of fused rings, but there is a trend: electron reorganization generally decreases with increased N . At $N = 24$, we observe that for the H-SiNC(6,4) and H-SiNC(4,6) structures, the change in the length in the armchair and zigzag directions significantly affects the electron and hole reorganization energies. The greatest decrease in λ_- and λ_+ is obtained from molecules with initial triplet spin multiplicity. Thus, these low reorganization energies indicate an advantage for the H-SiNCs to transport electrons or holes when coupled to an external device that either donates or withdraws electrons, such as a field-effect transistor [10]. Another observation from Table II is that λ_{\pm} follows the trend that larger clusters (more extended π conjugation) have smaller λ_{\pm} values. In the inset graph of Fig. 4, we illustrate the relationship between the EA and λ_- . It is observed that small H-SiNCs have low electron affinity and high electron reorganization energy. On the contrary, large H-SiNCs have high electron affinity and low electron reorganization energy, two important factors for good n -type materials [33]. In the case of linear or nearly linear H-SiNCs, Fig. 4(b) shows that the reorganization energy for all H-SiNCs decreases as N increases. This relation is comparable with the λN relation derived for linear oligomers [41], where N is the number of heterocyclic rings.

From our results, we observe that critical geometric changes of the neutral molecule can occur when an electron is added to the LUMO (λ_-) or when an electron it is removed from the HOMO (λ_+). The extra electron or hole in the neutral molecule induces localized charge defects in the form of polarons. The polaron binding energy is from the deformations in lattice and molecular geometries that

occur as the carrier localizes on a given site. This quantity is, thus, closely linked to the reorganization energy in electron-transfer theories. This polaron energy arising from internal degrees of freedom can be obtained by expanding the site energy ϵ_n in powers of molecular normal-mode coordinates, which can be calculated from the frontier molecular orbitals (HOMO and LUMO for hole and electron transport, respectively). In addition, these geometric changes among charge-transfer processes can correlate with the bonding character in the frontier orbitals [33]. This bonding character between two nearest atoms involving a molecular orbital is composed of bonding, antibonding, and nonbonding orbitals. For instance, adding an electron in the bonding orbital stabilizes the molecule because it is in between the atoms, while adding an electron into the antibonding orbital decreases the stability of the molecule. However, nonbonding involves only one atom, so the addition or removal of an electron does not change the energy or bond order (bond-length alteration) of the molecule. Interestingly, it has been demonstrated that by having a high nonbonding character [33], we can obtain low reorganization energies because nonbonding induces much less bond-length adjustment than bonding and antibonding upon charge transfer. Therefore, to examine whether structural adjustments with charge transfer correlate with the spatial distribution of frontier orbitals of the H-SiNCs to obtain low reorganization energies, we show in Fig. 5 that the percentage of nonbonding character is smaller in the HOMO than in the LUMO for H-SiNC(4,9) with an initial singlet state (see the Supplemental Material [31] for more information about bond-length alternations). Therefore, this factor should contribute to a larger value of λ_+ than λ_- . Comparing the height of the cation and anion for H-SiNC(4,9) with $S_{\text{initial}} = 0$, we observe that the height difference between the neutral and cation $|\Delta_{C-N}| = 0.005$ (Table I) is larger than that of $|\Delta_{A-N}| = 0.004$, as with the

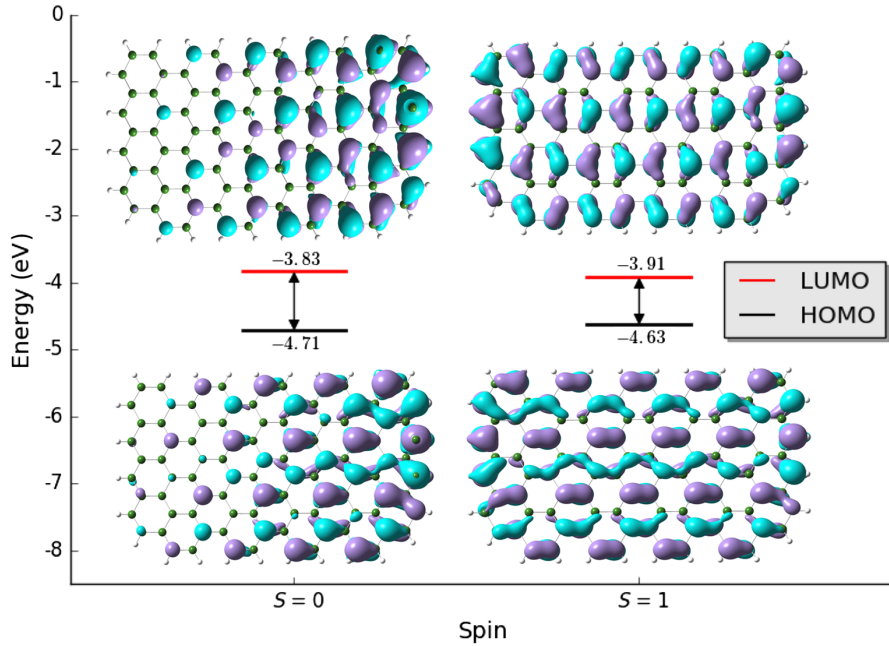


FIG. 5. Frontier orbitals for neutral H-SiNC(4,9) with initial singlet ($S = 0$) and triplet ($S = 1$) states at the B3LYP cc-pVDZ level of theory. Molecular orbitals are drawn with GaussView [32].

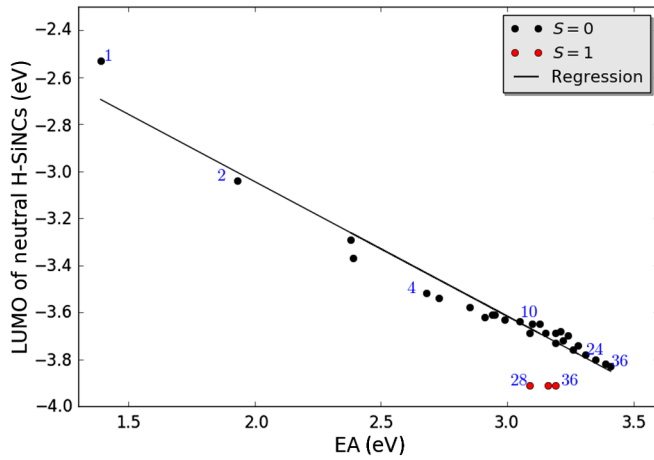


FIG. 6. Correlation of the computed EA for all H-SiNCs studied with the corresponding LUMO energy computed for the corresponding neutral H-SiNC. The numbers in the graph indicate the number of fused rings (N) for selected H-SiNCs. Here, S represents the triplet and singlet states for $S = 1$ and $S = 0$, respectively.

values of λ_+ relative to λ_- . In Fig. 5, it is shown that when more extended delocalization is present for the initial triplet-state molecule, the extended delocalization leads to the reduction of λ_+ and λ_- . For H-SiNC(4,9) with $S_{\text{initial}} = 1$ (see Fig. 5), it is noted that the values of $|\Delta_{A-N}| = 0.008$ are larger than that of $|\Delta_{C-N}| = 0.006$ (Table I), as with the values of λ_- relative to λ_+ . Therefore, this height difference shows how specific structural modifications such as bond-length alterations are originated upon the removal and addition of an electron to the silicene nanoclusters.

In Fig. 6, the calculated LUMO energy level versus electron affinity for all H-SiNCs is shown. The data show two different electronic configurations based on the initial

ground states of the neutral molecules. First, we observe that there is a correlation between the EA with the DFT-computed LUMO energies of the neutral species (E_{LUMO}) with the corresponding initial spin state having a linear regression of

$$E_{\text{LUMO}} = -0.573 \times \text{EA} - 1.89 \text{ eV}, \quad (5)$$

where both E_{LUMO} and EA are in electron volts. The average absolute error in this relationship is 0.052 eV. The trend shows that LUMO energy levels generally decrease with increased EA. In addition, it is noted that the EA increases as a function of the number of fused rings (N). These calculations indicate that both LUMO and EA can be independent to some extent, for instance, with respect to the number of fused rings.

IV. SUMMARY AND OUTLOOK

In this study, we show that low hole and electron reorganization energies of H-SiNCs can be obtained. The most straightforward way of reducing these reorganization energies is achieved by increasing the number of fused rings N . This is due to the extended π conjugation of H-SiNCs. It is further found that there exists an inverse dependence between the electron reorganization energy and the number of fused rings. Moreover, silicene nanoclusters are promising candidates as electron acceptors (n type) because they have high electron affinities and low reorganization energies for electron transfer, which result from a large conjugated system. EA and λ_- can be further optimized by extending conjugation either through increasing the size of the system or by picking a specific direction, i.e., zigzag or armchair. We can also conclude that

the spin state makes a significant change to the reorganization energy for corresponding silicene nanoclusters with $n_a > n_z$. In addition, the percentage of nonbonding character could play a crucial role in the internal reorganization. Therefore, understanding the charge-transport mechanism in terms of reorganization energies of these H-SiNCs is a key point for the design and stability of H-SiNCs electronic components.

Moreover, having explored the reduction of the reorganization energy through two methods, we suggest another strategy for reducing the reorganization energy: the application of constraints that prevents or minimizes the restructuring (distortions) along the vertical axes for the silicene nanoclusters. For instance, we can apply some constraints to the silicene nanocluster with the advantage of using atomically thin van der Waals materials and their ability to form heterostructures. This exploits the fact that these heterostructures can form junctions that are composed of p - and n -type semiconductors, each one being one unit cell thick, which exhibit completely different charge-transport characteristics than bulk heterojunctions [42]. Thus, we can realize a p - n junction by using individually contacted layers of p -type tungsten diselenide [43] and the n -type silicene nanoclusters to create an atomically thin p - n junction. This type of heterostructure needs to encapsulate the silicene nanoclusters within a rigid matrix that can avoid structural rearrangements. The encapsulation with other 2D materials such as graphene and h -BN layers can additionally avoid these silicene nanoclusters from becoming oxidized, as has been done for phosphorene [44]. Other effective ways to protect the silicene nanoclusters of oxidation are (i) using a nonreactive *in situ* capping procedure that protects the silicene nanocluster by means of reactive molecular beam deposition of Al_2O_3 [45], (ii) covering the silicene nanoclusters with polymers such as PMMA [46], and (iii) depositing metal ions on top of silicene nanoclusters, which can increase the stability and transistor performance of the silicene nanoclusters [47]. Finally, these types of systems may lead to unique material platforms of novel, high-performance electronic and optoelectronic devices.

ACKNOWLEDGMENTS

R. P.-P. is grateful to Roberto Olivares-Amaya for the discussion on reorganization energy in organic systems. M. D., J. K., and R. P.-P. acknowledge the King Abdullah University of Science and Technology for support under Contract (No. OSR-2015-CRG4-2634). H. L.-R. and S. F. acknowledge financial support from CONACyT (Grant No. 251684). J.-L. M.-C. start-up funds from Florida State University and the Energy and Material Initiative and facilities at the High Performance Material Institute. A portion of this work was performed at the National High Magnetic Field Laboratory, which is supported by

National Science Foundation Cooperative Agreement No. DMR-1644779* and the State of Florida.

APPENDIX: DFT APPROXIMATION

For the density-functional approach, we use the B3LYP functional because it provides good results compared with experimental data. For instance, we compare the bond-length alternation and torsional potentials using the results of disilane ($\text{H}_3\text{Si-SiH}_3$). This B3LYP functional also gives encouraging results for the average calculated nearest Si—Si distance for a silicene nanoribbon on Ag(110) (2.24 Å) [48]. Furthermore, we compare the results of disilane ($\text{H}_3\text{Si-SiH}_3$) using the B3LYP functional with others such as M062x and Perdew-Berke-Ernzerhof (PBE) functionals as shown in Table III.

Because of silicene's corrugated structure and due to B3LYP's inability to account for medium- and long-range electron noncovalent interactions, we think it is necessary to implement DFT $D3$ corrections to account for the intramolecular London forces, thereby possibly gaining non-negligible corrections to our systems' overall energy. These corrections are ultimately negligible in comparison to the systems' kinetic and potential energies, or otherwise, they are approximately the same for all cationic, anionic, and neutral nanoclusters of the same n_z and n_a dimensions canceling out whatever correction they might have while obtaining their respective relative energies, ionization potentials, and electronic affinities. As a result of the lack of importance of van der Waals corrections, we can, therefore, assume that our results are not affected by the artificial stabilization brought on by the basis-set superposition error.

Moreover, in order to evaluate dispersion effects and torsion around the Si—Si bond, we substitute the hydrogen atoms in the disilane molecule with the mesityl group (Mes) to obtain the disilene molecule ($\text{Mes}_2\text{Si} = \text{SiMes}_2$). The results are shown in Table IV. As can be seen from Table IV, the B3LYP functional gives results which are in

TABLE III. Experimental and computed results for disilane. The cc-pVDZ basis set is used for all functionals.

Type	Experiment	B3LYP	M062x	PBE
$d_{\text{Si-Si}}$ (Å)	2.331 [49]	2.358	2.348	2.357
$d_{\text{Si-H}}$ (Å)	1.492 [49]	1.497	1.491	1.51
$\angle\text{Si-Si-H}$	110.3° [50]	110.3°	110.2°	110.3°
$\angle\text{H-Si-H}$	108.6° [50]	108.7°	108.8°	108.6°

TABLE IV. Experimental and computational results for $\text{Mes}_2\text{Si} = \text{SiMes}_2$. The cc-pVDZ basis set is used for all functionals.

Type	Experiment	B3LYP	M062x	PBE
$d_{\text{Si-Si}}$ (Å)	2.16 [51]	2.16	2.14	2.19

TABLE V. Vertical ionization potential (IP_v) and the highest occupied molecular orbital energies (E_{HOMO}) at the B3LYP cc-pVDZ level for initial singlet states. Here, $DE = E_{\text{HOMO}} + IP_v$, where DE is the delocalization error in electron volts.

H-SiNC(n_z, n_a)	N	IP_v	E_{HOMO}	DE
(1,1)	1	7.28	-5.71	1.57
(2,1)	2	6.57	-5.28	1.29
(3,1)	3	6.14	-5.04	1.09
(4,1)	4	5.86	-4.96	0.89
(5,1)	5	5.71	-4.94	0.77
(6,1)	6	5.64	-4.93	0.71
(7,1)	7	5.61	-4.93	0.68
(2,2)	4	6.14	-5.07	1.07
(3,2)	6	5.81	-4.88	0.93
(4,2)	8	5.61	-4.88	0.73
(5,2)	10	5.53	-4.88	0.65
(6,2)	12	5.52	-4.90	0.62
(7,2)	14	5.53	-4.91	0.62
(3,3)	9	5.61	-4.83	0.78
(4,3)	12	5.46	-4.82	0.64
(5,3)	15	5.45	-4.84	0.61
(6,3)	18	5.47	-4.88	0.59
(7,3)	21	5.42	-4.86	0.56
(4,4)	16	5.37	-4.79	0.58
(5,4)	20	5.39	-4.83	0.56
(6,4)	24	5.43	-4.84	0.59
(7,4)	28	5.33	-4.80	0.53
(4,5)	20	5.30	-4.76	0.54
(4,6)	24	5.26	-4.75	0.51
(4,7)	28	5.22	-4.73	0.49
(4,8)	32	5.18	-4.72	0.46
(4,9)	36	5.30	-4.71	0.59

good agreement with the experimental results. Consequently, the B3LYP functional is chosen for geometrical optimizations of our silicene nanoclusters. The B3LYP functional also shows that the torsional effect is not very significant for the cc-pVDZ basis, which has no diffuse functions. Therefore, computations on anions without using the diffuse functions cannot change the results for our systems. Additionally, the introduction of diffuse functions markedly increases the computational cost of the electronic structure methods and increases the convergence difficulties.

In addition, to prove that our conclusions are not entirely dependent on the type of functional selected, we try to compare the results of B3LYP with different long-range corrected functionals. Then, we calculate the reorganization energies and adiabatic ionization potential as well as the adiabatic electronic affinity with different systems and different functionals to show that these values are not totally dependent on the functional used.

Usually long-range corrected (LRC) functionals are commonly used to enforce the computed molecular IP to be equal to the negative energy of the HOMO of the neutral molecules ($-E_{\text{HOMO}}$), i.e., $r^{-1} = r^{-1}[1 - \text{erf}(\omega r)] + r^{-1}\text{erf}(\omega r)$. However, setting ω to a fixed value is an

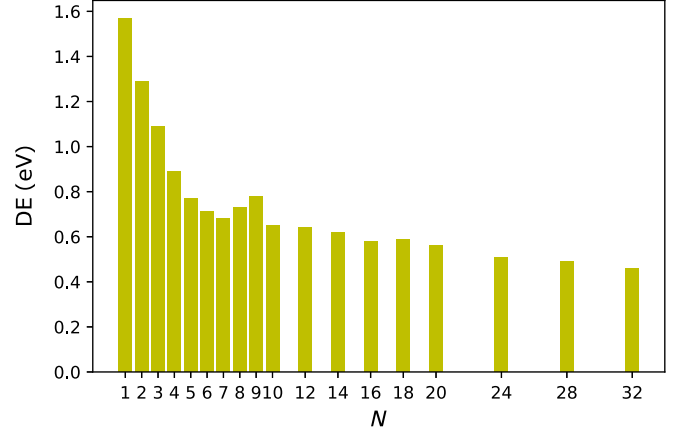


FIG. 7. Deviations between the calculated E_{HOMO} and IP_v for a series of selected H-SiNCs from Table S4 in the Supplemental Material [31].

approximation in itself, as ω is a functional of the electron density [52]. Thereby, choosing the correct value of ω as well as a LRC functional is nontrivial, as ω strongly depends on the system under study [52,53]. Moreover, the value of ω that is optimal for ground-state properties may not necessarily be optimal for excited-state properties [52,54]. The criterion that LRC functionals should satisfy the known Koopman's theorem is given by [55]

$$-E_{\text{HOMO}}(\omega) = IP_v(\omega) \equiv E(N-1; \omega) - E(N; \omega), \quad (\text{A1})$$

where E_{HOMO} is the HOMO energy for a specific choice of ω , and IP is the ionization potential of an N electron system.

In Table V, we compute the delocalization error using Eq. (A1) at the B3LYP cc-pVDZ level of theory. As can be seen, the delocalization error decreases with system size. Figure 7 illustrates the evolution of error in a series of selected nanoclusters from Table II. As the silicene nanocluster grows from $N = 1$ to $N = 32$, the E_{HOMO} gradually approaches the calculated negative vertical ionization potential (IP_v), leading to a smaller error bar than for $N = 1$.

To obtain an idea about the effect of the LRC functionals in our silicene nanoclusters, we use two typical values of ω (in a.u.⁻¹), which are $\omega = 0.33$ as in Refs. [56,57] and $\omega = 0.5$ as in Refs. [58,59]. We consider two hybrids of PBE functional since PBE functional seem to benefit the most from an admixture of Hartree-Fock (HF) exchange [60]. In addition, we use the Coulomb-attenuating method (CAM) B3LYP functional which combines the hybrid qualities of B3LYP and the long-range correction presented by Tawada *et al.* [56]. The value of ω is 0.33, which according to Tsuneda and co-workers gives improved results [56,57].

The numerical results are computed in Q-CHEM version 5.0 [61] and the Gaussian 16 electronic structure program. TURBOMOLE (7.1) is not used for the long-range corrected functionals because its library does not contain them. We indicate which calculations are performed in Q-CHEM, Gaussian,

TABLE VI. Computed results for H-SiNC(1,1), H-SiNC(5,1), and H-SiNC(4,6). The cc-pVDZ basis set is used for all functionals. Here, the delocalization errors are given as the absolute value of $DE = |E_{\text{HOMO}}(\omega) + \text{IP}_v(\omega)|$. All results are given in electron volts.

Type	Functional	λ_+	E_{HOMO}	IP	IP_v	DE
H-SiNCs(1,1) (Turbo7)	B3LYP	0.303	-5.71	7.12	7.28	1.57
H-SiNCs(1,1) (Q-CHEM5)	PBE	0.298	-5.34	7.24	7.39	2.06
H-SiNCs(1,1) (Q-CHEM5)	LRC ω PBE ($\omega = 0.5$)	0.260	-7.95	7.23	7.38	0.57
H-SiNCs(1,1) (Q-CHEM5)	LRC ω PBE ($\omega = 0.3$)	0.240	-7.66	7.24	7.36	0.30
H-SiNCs(1,1) (Q-CHEM5)	LRC ω PBEh ($\omega = 0.3$)	0.245	-8.32	7.74	7.87	0.45
H-SiNCs(1,1) (Q-CHEM5)	CAM B3LYP	0.256	-6.77	7.14	7.28	0.513
H-SiNCs(5,1) (Turbo7)	B3LYP	0.099	-4.94	5.66	5.71	0.77
H-SiNCs(5,1) (Q-CHEM5)	B3LYP	0.140	-4.88	5.70	5.76	0.88
H-SiNCs(5,1) (Turbo7)	PBE	0.096	-4.64	5.74	5.79	1.14
H-SiNCs(5,1) (Q-CHEM5)	PBE	0.099	-4.63	5.73	5.79	1.16
H-SiNCs(5,1) (Q-CHEM5)	LRC ω PBE ($\omega = 0.3$)	0.179	-6.32	5.74	5.83	0.49
H-SiNCs(5,1) (Q-CHEM5)	CAM B3LYP	0.220	-5.56	5.60	5.70	0.14
H-SiNCs(4,6) (Turbo7)	B3LYP	0.065	0.287	5.22	3.31	0.514
H-SiNCs(4,6) (Gaus16)	CAM B3LYP	0.097	-5.865	5.87	5.92	0.05

and TURBOMOLE with the following labels Q-CHEM5, Gaus16, and Turbo7, respectively.

We notice that there are a few changes in the values of the reorganization energies using TURBOMOLE (7.1) and Q-CHEM (5.0) at the same level of calculation (B3LYP cc-pVDZ). This is because the implementation of the B3LYP exchange-correlation functional has the form of $0.8 \text{ S} + 0.72 \text{ B88} + 0.2 \text{ HF} + 0.19 \text{ VWN(V)} + 0.81 \text{ LYP}$ in TURBOMOLE (7.1), which is the same functional form in the Gaussian program. In the case of Q-CHEM [61], the B3LYP exchange-correlation functional has the form of $0.080 \text{ S} + 0.72 \text{ B88} + 0.2 \text{ HF} + 0.19 \text{ VWN1RPA} + 0.81 \text{ LYP}$. Notice the difference for VWN(V) and VWN1RPA .

The comparison between the values obtained from B3LYP with those obtained with PBE are shown Table VI. Both values are very similar. By comparing the B3LYP with the LRC ω PBE calculations at two different values of ω , we observe that the LRC ω PBE reorganization energies are higher than the ones obtained with B3LYP. However, the HOMO energies E_{HOMO} s are larger than the IPs. This indicates that adding more long-range exact exchange than necessary by optimally tuning for Koopmans's theorem leads to a HOMO energy higher than the IP (sometimes called the localization error of HF), which is also observed in the localization error. In addition, we find that for LRC ω PBE, tuning ω in order to make $\text{IP} = -E_{\text{HOMO}}$ leads to an ω that decreases with increasing system size, meaning that less exact exchange can be used for larger molecules as done in other previous studies [62,63]. The exact exchange can also be explained in terms of electron delocalization; electron delocalization increases along with molecule size, necessitating a smaller weight of exact exchange.

However, we note that when using CAM B3LYP for H-SiNCs(5,1), we obtain a much higher hole reorganization energy than with LRC ω PBE (Q-CHEM5) and B3LYP

(Q-CHEM5). Noting that the delocalization error is smaller than 0.77 for the B3LYP cc-pVDZ level. A possible caveat is that we cannot determine if this difference comes from the implementation of B3LYP in Q-CHEM. To remove this doubt, we test a larger nanocluster H-SiNCs(4,6) in Gaussian 16. We use Gaussian 16 in this part because B3LYP is implemented in the same way as in TURBOMOLE 7.1. As we see in this case, the hole reorganization energies are in the same value range with a delocalization error close to zero. In addition, spin contamination is a problem when we include the long-range corrected part. For instance, the spin contamination S^2 of the radical cation of H-SiNCs(5,1) is 1.25 and 1.18 for CAM B3LYP (Q-CHEM5) and LRC ω PBE (Q-CHEM5), respectively. This problem is minor for the B3LYP functional with $S^2 = 0.801$, which deviates only by 0.051 with the exact value $S^2 = 0.750$ [31]. The value of spin contamination for H-SiNCs(4,6) is $S^2 = 3.37$ for CAM B3LYP (Gaus16) indicating that the wave function is mixing with a triplet state (see Ref. [31]).

While Eq. (A1) is shown to be useful for determining IPs, we can also adapt Koopmans's theorem for computing the EA for the IP of the $N + 1$ electron system. In the case of using ω , which minimizes the overall derivation expressed in the target function, we use the following expression [62]:

$$J(\omega) = |E_{\text{HOMO}}(N, \omega) + \text{IP}(N, \omega)| + |E_{\text{HOMO}}(N + 1, \omega) + \text{IP}(N + 1, \omega)|. \quad (\text{A2})$$

The downside of using Eq. (A2) is that the optimal value of ω needs to be determined for each system of interest separately. The $\text{IP}(N + 1)$ can be related with the EA of an N electron system.

Using Eq. (8), we compute J for the EAs in the respective silicene nanoclusters presented in Table VII. According to

TABLE VII. Computed results for H-SiNC(1,1), H-SiNC(5,1), and H-SiNC(4,6). The cc-pVDZ basis set is used for all functionals. All results are given in electron volts.

Type	Functional	λ_-	$E_{\text{HOMO}}(N+1)$	$\text{IP}(N+1)$	J	DE
H-SiNCs(1,1) (Turbo7)	B3LYP	0.775	-0.253	1.39	2.71	1.57
H-SiNCs(1,1) (Q-CHEM5)	PBE	0.853	-0.038	1.60	3.62	2.06
H-SiNCs(1,1) (Q-CHEM5)	LRC ω PBE	1.59	-2.99	1.80	1.77	0.57
	($\omega = 0.5$)					
H-SiNCs(1,1) (Q-CHEM5)	LRC ω PBEh	1.51	-3.08	1.95	1.58	0.45
	($\omega = 0.3$)					
H-SiNCs(5,1) (Turbo7)	B3LYP	0.088	-2.10	2.85	1.52	0.77
H-SiNCs(5,1) (Q-CHEM5)	B3LYP	0.129	-2.18	2.99	1.70	0.88
H-SiNCs(5,1) (Turbo7)	PBE	0.091	-1.98	3.09	2.26	1.14
H-SiNCs(5,1) (Q-CHEM5)	PBE	0.093	-1.98	3.09	2.27	1.16
H-SiNCs(5,1) (Q-CHEM5)	LRC ω PBE	0.296	-3.68	3.14	1.02	0.49
	($\omega = 0.3$)					
H-SiNCs(5,1) (Q-CHEM5)	CAM B3LYP	0.440	-2.95	3.07	0.25	0.14
H-SiNCs(4,6) (Turbo7)	B3LYP	0.287	-2.82	3.31	1.00	0.514
H-SiNCs(4,6) (Gaus16)	CAM B3LYP	0.496	-3.22	2.93	0.34	0.05

Table VII, pure density-functional approximations B3LYP and PBE predict more positive HOMO energies in anions than LRC functionals, which can be seen by observing the $E_{\text{HOMO}}(N+1)$. Adding a certain amount of HF exchange makes all occupied orbital energies more negative. However, the J error is larger than delocalization error, meaning that the EAs seem not to benefit at all from the admixture of the exact HF exchange, especially for the larger silicene nanocluster H-SiNCs(4,6) as shown in Table VII. When a finite basis set is used, the highest occupied orbital seems artificially stabilized irrespective of the value and sign of the orbital eigenvalue. This is the success of the density-functional approximations in predicting EAs, which seems to rest on basis-set effects and error cancellations, which do not necessarily comply with theoretical justifications for our case.

In conclusion, we demonstrate that the results obtained with the B3LYP functional are not artifacts after comparing the results with some LRC functionals. The results shown in Tables VI and VII demonstrate that the error in IPs can be slightly reduced only by using a long-corrected functional. For EAs, an admixture of HF exchange in any form increases the error.

- [1] F. Xia, D. B. Farmer, Y. M. Lin, and P. Avouris, Graphene field-effect transistors with high on/off current ratio and large transport band gap at room temperature, *Nano Lett.* **10**, 715 (2010).
- [2] L. G. De Arco, Y. Zhang, C. W. Schlenker, K. Ryu, M. E. Thompson, and C. Zhou Continuous, highly flexible, and transparent graphene films by chemical vapor deposition for organic photovoltaics, *ACS Nano* **4**, 2865 (2010).

- [3] S. S. Varghese, S. Lonkar, K. K. Singh, S. Swaminathan, and A. Abdala, Recent advances in graphene based gas sensors, *Sens. Actuator B Chem.* **218**, 160 (2015).
- [4] R. Raccichini, A. Varzi, S. Passerini, and B. Scrosati, The role of graphene for electrochemical energy storage, *Nat. Mater.* **14**, 271 (2015).
- [5] J. Qiao, X. Kong, Z.-X. Hu, F. Yang, and W. Ji, High-mobility transport anisotropy and linear dichroism in few-layer black phosphorus, *Nat. Commun.* **5**, 4475 (2014).
- [6] B. Radisavljevic, A. Radenovic, J. Brivio, V. Giacometti, and A. Kis Single-layer MoS₂ transistors, *Nat. Nanotechnol.* **6**, 147 (2011).
- [7] S. Cahangirov, M. Topsakal, E. Akturk, H. Sahin, and S. Ciraci, Two- and One-Dimensional Honeycomb Structures of Silicon and Germanium, *Phys. Rev. Lett.* **102**, 236804 (2009).
- [8] R. Pablo-Pedro, H. Lopez-Rios, S. Fomine, and M. S. Dresselhaus, Detection of multiconfigurational states of hydrogen-passivated silicene nanoclusters, *J. Phys. Chem. Lett.* **8**, 615 (2017).
- [9] Y. Ding and J. Ni, Electronic structures of silicon nanoribbons, *Appl. Phys. Lett.* **95**, 083115 (2009).
- [10] L. Tao, E. Cinquanta, D. Chiappe, C. Grazianetti, M. Fanciulli, M. Dubey, A. Molle, and D. Akinwande, Silicene field-effect transistors operating at room temperature, *Nat. Nanotechnol.* **10**, 227 (2015).
- [11] Y. Wang, J. Zheng, Z. Ni, R. Fei, Q. Liu, R. Quhe, C. Xu, J. Zhou, Z. Gao, and J. Lu, Half-metallic silicene and germanene nanoribbons: Towards high-performance spintronics device, *Nano* **7**, 1250037 (2012).
- [12] W. L. Wang, S. Meng, and E. Kaxiras, Graphene nanoflakes with large spin, *Nano Lett.* **8**, 244 (2008).
- [13] L. C. Campos, V. R. Manfrinato, J. D. Sanchez-Yamagishi, J. Kong, and P. Jarillo-Herrero, Anisotropic etching and nanoribbon formation in single-layer graphene, *Nano Lett.* **9**, 2600 (2009).
- [14] J. H. Schön, C. Kloc, and B. Batlogg, Universal Crossover from Band to Hopping Conduction in Molecular Organic Semiconductors, *Phys. Rev. Lett.* **86**, 3843 (2001).

- [15] J. L. Bredas, J. P. Calbert, D. A. da Silva Filho, and J. Cornil, Organic semiconductor: A theoretical characterization of the basic parameters governing charge transport, *Proc. Natl. Acad. Sci. U.S.A.* **99**, 5804 (2002).
- [16] N. M. Oboyle, C. M. Campbell, and G. R. Hutchison, Computational design and selection of optimal organic photovoltaic materials, *J. Phys. Chem. C* **115**, 16200 (2011).
- [17] G. R. Hutchison, M. A. Ratner, and T. J. Marks, Intermolecular charge transfer between heterocyclic oligomers. Effects of heteroatom and molecular packing on hopping transport in organic semiconductors, *J. Am. Chem. Soc.* **127**, 16866 (2005).
- [18] A. Devos and M. Lannoo, Electron-phonon coupling for aromatic molecular crystals: Possible consequences for their superconductivity, *Phys. Rev. B* **58**, 8236 (1998).
- [19] J.-L. Brédas, D. Beljonne, V. Coropceanu, and J. Cornil Charge-transfer and energy-transfer processes in pi-conjugated oligomers and polymers: A molecular picture, *Chem. Rev.* **104**, 4971 (2004).
- [20] J. C. Sancho-García and A. J. Pérez-Jiménez, Charge-transport properties of prototype molecular materials for organic electronics based on graphene nanoribbons, *Phys. Chem. Chem. Phys.* **11**, 2741 (2009).
- [21] S. Larsson, A. Klimkans, L. Rodriguez-Monge, and G. Duskesas, Reorganization energies in organic pi systems, *J. Mol. Struct.* **425**, 155 (1998).
- [22] Y.-P. Sun, P. Wang, and N. B. Hamilton, Fluorescence spectra and quantum yields of buckminsterfullerene (C60) in room-temperature solutions. No excitation wavelength dependence?, *J. Am. Chem. Soc.* **115**, 6378 (1993).
- [23] V. Coropceanu, M. Malagol, D. A. da Silva Filho, N. E. Gruhn, T. G. Bill, and J. L. Bredas, Hole- and Electron-Vibrational Couplings in Oligoacene Crystals: Intramolecular Contributions, *Phys. Rev. Lett.* **89**, 275503 (2002).
- [24] M. Xu, T. Liang, M. Shi, and H. Chen, Graphene-like two-dimensional materials, *Chem. Rev.* **113**, 3766 (2013).
- [25] Q. H. Wang, K. Kalantar-Zadeh, A. Kis, J. N. Coleman, and M. S. Strano, Electronics and optoelectronics of two-dimensional transition metal dichalcogenides, *Nat. Nanotechnol.* **7**, 699 (2012).
- [26] X. Ling, H. Wang, S. Huang, F. Xia, and M. S. Dresselhaus, The renaissance of black phosphorus, *Proc. Natl. Acad. Sci. U.S.A.* **112**, 4523 (2015).
- [27] A. N. Rudenko, S. Brener, and M. I. Katsnelson, Intrinsic Charge Carrier Mobility in Single-Layer Black Phosphorus, *Phys. Rev. Lett.* **116**, 246401 (2016).
- [28] S. Grimme, J. Antony, S. Ehrlich, and H. Krieg, A consistent and accurate *ab initio* parametrization of density functional dispersion correction (DFT-D) for the 94 elements H-Pu, *J. Chem. Phys.* **132**, 154104 (2010).
- [29] L. Noodleman, Valence bond description of antiferromagnetic coupling in transition metal dimers, *J. Chem. Phys.* **74**, 5737 (1981).
- [30] A. Alrichs, F. Furche, C. Hättig, W. Klopper, M. Sierka, and F. Weigend, TURBOMOLE v7.0, University of Karlsruhe and Forschungszentrum Karlsruhe GmbH, 2015 [<http://www.turbomole.com>].
- [31] See Supplemental Material at <http://link.aps.org/supplemental/10.1103/PhysRevApplied.9.054012> for CASSCF calculations for the system that presents an initial triplet state. In addition, a detailed discussion of the spin contamination for the cations and anions is given.
- [32] M. J. Frisch, G. W. Trucks, H. B. Schlegel, G. E. Scuseria, M. A. Robb, J. R. Cheeseman, G. Scalmani, V. Barone, B. Mennucci, G. A. Petersson, H. Nakatsuji, M. Caricato, X. Li, H. P. Hratchian, A. F. Izmaylov, J. Bloino, G. Zheng, and D. J. Sonnenb, Gaussian 16, revision D.01, Gaussian, Inc., 2013.
- [33] Y. C. Chang and I. Chao, An important key to design molecules with small internal reorganization energy: Strong nonbonding character in frontier orbitals, *J. Phys. Chem. Lett.* **1**, 116 (2010).
- [34] N. E. Gruhn, D. A. da Silva Filho, T. G. Bill, M. Malagoli, V. Coropceanu, A. Kahn, and J.-L. Brédas The vibrational reorganization energy in pentacene: Molecular influences on charge transport, *J. Am. Chem. Soc.* **124**, 7918 (2002).
- [35] X. Amashukeli, J. R. Winkler, H. B. Gray, N. E. Gruhn, and D. L. Lichtenberger, Electron-transfer reorganization energies of isolated organic molecules, *J. Phys. Chem. A* **106**, 7593 (2002).
- [36] Jonathan C. Rienstra-Kiracofe, Gregory S. Tschumper, and Henry F. Schaefer, Atomic and molecular electron affinities: Photoelectron experiments and theoretical computations, *Chem. Rev.* **102**, 231 (2002).
- [37] M. Y. Kuo, H. Y. Chen, and I. Chao, Cyanation: Providing a three-in-one advantage for the design of *n*-type organic field-effect transistors, *Chem. Eur. J.* **13**, 4750 (2007).
- [38] Y.-C. Chang, M.-Y. Kuo, C.-P. Chen, H.-F. Lu, and I. Chao, On the air stability of *n*-channel organic field-effect transistors: A theoretical study of adiabatic electron affinities of organic semiconductors, *J. Phys. Chem. C* **114**, 11595 (2010).
- [39] C. R. Newman, C. D. Frisbie, A. Demetrio, S. Filho, and J. Bre, Introduction to organic thin film transistors and design of *n*-channel organic semiconductors, *Chem. Mater.* **16**, 4436 (2004).
- [40] A. Facchetti, M. H. Yoon, C. L. Stern, H. E. Katz, and T. J. Marks, Building blocks for *n*-type organic electronics: Regiochemically modulated inversion of majority carrier sign in perfluoroarene-modified polythiophene semiconductors, *Angew. Chem., Int. Ed. Engl.* **42**, 3900 (2003).
- [41] S. S. Zade and M. Bendikov, Study of hopping transport in long oligothiophenes and oligoselenophenes: Dependence of reorganization energy on chain length, *Chem. Eur. J.* **14**, 6734 (2008).
- [42] C.-H. Lee *et al.* Atomically thin *p-n* junctions with van der Waals heterointerfaces, *Nat. Nanotechnol.* **9**, 676 (2014).
- [43] X. Yu, M. S. Prévot, N. Guijarro, and K. Sivula, Self-assembled 2D WSe₂ thin films for photoelectrochemical hydrogen production, *Nat. Commun.* **6**, 7596 (2015).
- [44] L. Li *et al.* Direct observation of the layer-dependent electronic structure in phosphorene, *Nat. Nanotechnol.* **12**, 21 (2017).
- [45] A. Molle, C. Grazianetti, D. Chiappe, E. Cinquanta, E. Ciani, G. Tallarida, and M. Fanciulli Hinderling the oxidation of silicene with non-reactive encapsulation, *Adv. Funct. Mater.* **23**, 4340 (2013).
- [46] S. P. Koenig, R. A. Doganov, H. Schmidt, A. H. Castro Neto, and B. Özyilmaz, Electric field effect in ultrathin black phosphorus, *Appl. Phys. Lett.* **104**, 103106 (2014).

- [47] Z. Guo, S. Chen, Z. Wang, Z. Yang, F. Liu, Y. Xu, J. Wang, Y. Yi, H. Zhang, L. Liao, P. K. Chu, and X.-F. Yu, Metal-ion-modified black phosphorus with enhanced stability and transistor performance, *Adv. Mater.* **29**, 1703811 (2017).
- [48] B. Aufray, A. Kara, S. Vizzini, H. Oughaddou, C. Léandri, B. Ealet, and G. L. Lay Graphene-like silicon nanoribbons on Ag(110): A possible formation of silicone, *Appl. Phys. Lett.* **96**, 183102 (2010).
- [49] E. L. Eliel, *Stereochemistry of Organic Compounds* (Wiley, New York, 2001).
- [50] K. I. Dahlqvist and S. Forsén, The barrier to internal rotation in 2-furaldehyde, *J. Phys. Chem.* **69**, 4062 (1965).
- [51] G. Raabe and J. Michl, Multiple bonding to silicon, *Chem. Rev.* **85**, 419 (1985).
- [52] R. Baer, E. Livshits, and U. Salzner, Tuned range-separated hybrids in density functional theory, *Annu. Rev. Phys. Chem.* **61**, 85 (2010).
- [53] R. Baer and D. Neuhauser Density Functional Theory with Correct Long-Range Asymptotic Behavior, *Phys. Rev. Lett.* **94**, 043002 (2005).
- [54] M. A. Rohrdanz, K. M. Martins, and J. M. Herbert, A long-range-corrected density functional that performs well for both ground-state properties and time-dependent density functional theory excitation energies, including charge-transfer excited states, *J. Chem. Phys.* **130**, 054112 (2009).
- [55] N. Kuritz, T. Stein, R. Baer, and L. Kronik, Charge-transfer-like $\pi \rightarrow \pi^*$ excitations in time-dependent density functional theory: A conundrum and its solution, *J. Chem. Theory Comput.* **7**, 2408 (2011).
- [56] Y. Tawada, T. Tsuneda, S. Yanagisawa, T. Yanai, and K. Hirao, A long-range-corrected time-dependent density functional theory, *J. Chem. Phys.* **120**, 8425 (2004).
- [57] M. Kamiya, T. Tsuneda, and K. Hirao, A density functional study of van der Waals interactions, *J. Chem. Phys.* **117**, 6010 (2002).
- [58] I. C. Gerber and J. G. Ángyán, Hybrid functional with separated range, *Chem. Phys. Lett.* **415**, 100 (2005).
- [59] J. G. Lngyaln, I. C. Gerber, A. Savin, and J. Toulouse, Van der Waals forces in density functional theory: Perturbational long-range electron-interaction corrections, *Phys. Rev. A* **72**, 012510 (2005).
- [60] M. Ernzerhof and G. E. Scuseria, Assessment of the Perdew-Burke-Ernzerhof exchange-correlation functional, *J. Chem. Phys.* **110**, 5029 (1999).
- [61] Y. Shao *et al.* Advances in molecular quantum chemistry contained in the Q-CHEM 4 program package, *Mol. Phys.* **113**, 184 (2015).
- [62] T. Stein, H. Eisenberg, L. Kronik, and R. Baer, Fundamental Gaps in Finite Systems from Eigenvalues of a Generalized Kohn-Sham Method, *Phys. Rev. Lett.* **105**, 266802 (2010).
- [63] U. Salzner and A. Aydin, Improved prediction of properties of π -conjugated oligomers with range-separated hybrid density functionals, *J. Chem. Theory Comput.* **7**, 2568 (2011).